Uncatalyzed Transfer Hydrogenation of Quinones and Related Systems: A Theoretical Mechanistic Study

Bun Chan* and Leo Radom*

School of Chemistry and Centre of Excellence in Free Radical Chemistry and Biotechnology, University of Sydney, Sydney, NSW 2006, Australia

Quantum chemistry calculations have been used to study the uncatalyzed transfer hydrogenation between a range of hydrogen donors and acceptors, in the gas phase and in solution. Our study shows in the first place that in order to obtain reliable condensed-phase transition structures, it is necessary to perform geometry optimization in the presence of a continuum. In addition, the use of a free energy of solvation obtained with the UB3-LYP/6-31+G(d,p)/IEF-PCM/UA0 combination, in conjunction with UMPWB1K/6-311+G(3df,-2p)//B3-LYP/6-31+G(d,p) gas-phase energies, gives the best agreement with experimental barriers. In condensed phases, the geometries and energies of the transition structures are found to relate to one another in a manner consistent with the Hammond postulate. There is also a correlation between the barriers and the energies of the radical intermediates in accord with the Bell−Evans−Polanyi principle. We find that in the gas phase, all the transfer-hydrogenation reactions examined proceed via a radical pathway. In condensed phases, some of the reactions follow a radical mechanism regardless of the solvent. *However, for some reactions there is a change from a radical mechanism to an ionic mechanism as the solvent becomes more polar.* Our calculations indicate that the detection of radical adducts by EPR does not necessarily indicate a predominant radical mechanism, because of the possibility of a concurrent ionic reaction. We also find that the transition structures for these reactions do not necessarily have a strong resemblance to the intermediates, and therefore one should be cautious in utilizing the influence of polar effects on the rate of reaction as a means of determining the mechanism.

1. Introduction

Transfer hydrogenations are reactions that involve a net transfer of two hydrogen atoms from a donor molecule to an acceptor containing unsaturated bonds (e.g., C=C, C=O, or C=N).[1] These reactions play a vital role in coal liquefaction, aromatization reactions with nitroarenes or quinones, and possibly biochemical dehydrogenations.[2] In contrast to conventional transition-metal-catalyzed hydrogenation reactions,[3] transfer hydrogenations may be carried out in the absence of metals by employing high temperatures. Such conditions are naturally attractive, as they offer an environmentally benign alternative to present industrial methods of hydrogenation. A large variety of compounds with weakly bound hydrogen atoms can be employed as H-donors, in conjunction with a broad range of H-acceptors such as alkenes, ketones, polycyanoalkenes, quinones, and molecules containing nitro or nitroso groups, making transfer hydrogenation a versatile reaction. Indeed, this type of reaction has been recently identified as a potential prototype for the process of coherently controlled racemic purification.[4]

A typical example of transfer hydrogenation is provided by the condensed-phase reaction between acridan (ACD) and α-methylstyrene (AMS), which gives acridine and isopropylbenzene.[5] Two of the more probable mechanisms are hydrogen atom transfer (pathway A) and hydride transfer (pathway B), as shown in reaction 1. Based on the minimal polar substituent effects observed, it was proposed that the transfer hydrogenation

(1)
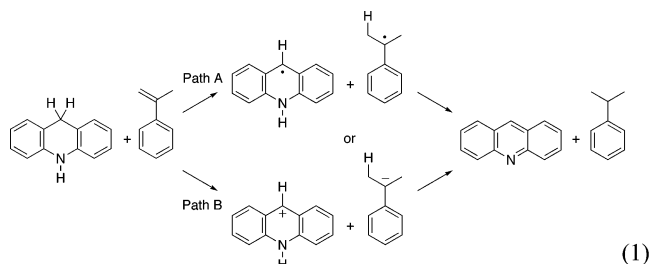
of acridan with α-methylstyrene proceeds via the biradical pathway (pathway A).

Likewise, based on observed pressure effects and density functional theory (DFT) calculations, the transfer-hydrogenation reactions of hydroaromatic compounds with benzoquinones, e.g., the transfer hydrogenation between 1,4-cyclohexadiene (CHD) and 2,3-dichloro-5,6-dicyano-1,4-benzoquinone (DDQ), are also believed to proceed via a biradical mechanism (reaction 2).[6]

(2)
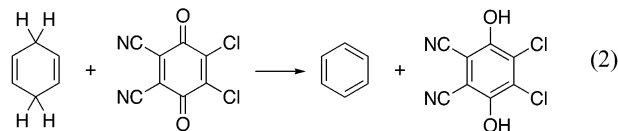
On the other hand, there have been numerous reports dealing with the same type of reaction (i.e., hydroaromatic compounds with benzoquinones) in which an ionic mechanism has been proposed,[7] whereby the mechanism involves a transfer of hydride (rather than a hydrogen atom) to the quinone oxygen, followed by a proton transfer (i.e., pathway B). As part of a

* Address correspondence to this author. E-mail: chan_b@chem.usyd.edu.au; radom@chem.usyd.edu.au.

Study of Uncatalyzed Transfer Hydrogenation

J. Phys. Chem. A, Vol. 111, No. 28, 2007 **6457**

Figure 1. Acronyms for hydrogen donors and hydrogen acceptors.

continuing investigation,[8] we have been interested in pursuing the fundamentals of transition-metal-free hydrogenation. In the present paper, we address the question of when does a transfer-hydrogenation reaction proceed via a radical pathway and when does it proceed via an ionic pathway, using density functional theory (DFT) calculations. The reactions shown as 1 and 2 above, as well as the additional reactions 3−6, are examined as representative examples of transfer-hydrogenation reactions.

Reactions 1, 2, 5, and 6 involving systems of moderate size are investigated in detail, while reactions 3 and 4 involving larger systems are studied less fully. The hydrogen donors and acceptors examined, together with their acronyms, are displayed in Figure 1.

2. Theoretical Procedures

Standard density functional theory calculations[9] were carried out with the GAUSSIAN 03 program.[10] Geometries were optimized at the B3-LYP/6-31+G(d,p) level of theory. The intrinsic reaction coordinate (IRC) method was employed to confirm that each transition structure is linked to the appropriate adjacent minima. Improved relative energies were obtained with MPWB1K[11] with the 6-311+G(3df,2p) basis set. It has been found that, for prototypical transfer-hydrogenation reactions, geometries and energies obtained at these levels yield relative energies that are comparable to those obtained from high-level single- and multireference ab initio methods.[8g]

Because the transition structures potentially involve biradicals, this leads to a multireference problem whose solution requires a satisfactory account of nondynamical correlation. It has been shown that unrestricted broken-symmetry (UBS, denoted U hereafter for simplicity) DFT procedures perform surprisingly well in such situations.[12] This has been attributed to the implicit and explicit inclusion of nondynamical correlation effects in UDFT via the form of the exchange-correlation functional. In the present study, geometry optimizations, frequencies, and

single-point energy calculations were carried out with both restricted (R) and unrestricted (U) methods. We find that UMPWB1K single-point energies are always significantly lower than the corresponding RMPWB1K values. This is consistent with our previous finding that in the transfer hydrogenation between ethane and ethene,[8g] RDFT procedures lead to substantially higher barriers when compared with high-level ab initio values, while the UDFT barriers are comparable to the high-level ab initio barriers. Consequently, unless otherwise noted, barriers reported in the text are those corresponding to UMPWB1K single-point energies for the transition structures.

In wave function-based methods such as Hartree−Fock, an unrestricted solution of the wave function contains contributions from higher spin states, predominantly the state of next highest multiplicity, e.g., for a singlet, the unrestricted wave function normally shows some triplet character. The degree of spin contamination for a ground-state singlet can serve as a qualitative indication of the extent of biradical character, because it largely reflects the contribution from the biradical triplet state. A measure of the degree of spin contamination is in turn given by the deviation in the expectation value of the spin-squared operator, $\langle S^2 \rangle$, from the value for a pure spin state.[13] The value of $\langle S^2 \rangle$ would be 0 for a pure singlet and 2 for a pure triplet. For UDFT methods, it has been argued that $\langle S^2 \rangle$ in the Kohn−Sham wave function is not well defined.[14] However, efforts to calculate $\langle S^2 \rangle$ for UDFT based on methods such as the Löwdin formula[15] and the spin magnetization density[16] have yielded results consistent with the $\langle S^2 \rangle$ values obtained from the KS orbitals. It has thus been concluded that, while $\langle S^2 \rangle$ values calculated from the KS orbitals may not be formally correct, they are still reasonably meaningful and contain relevant information. Therefore, KS $\langle S^2 \rangle$ values are used in the present study as a means of indicating the extent of biradical character in the transition structures. A strictly ionic TS would have an $\langle S^2 \rangle$ value of zero, while a TS with biradical character would have a nonzero $\langle S^2 \rangle$.

In addition to the major contribution from relative energies at 0 K, relative free energies at finite temperatures include thermal corrections to enthalpies (H_{temp}) and absolute entropies (S), which we have obtained from B3-LYP/6-31+G(d,p) frequencies (298 K and 1 M, unless otherwise noted). Literature scale factors[17] were used in the evaluation of the zero-point vibrational energies (ZPVE), enthalpies, and entropies from the B3-LYP/6-31+G(d,p) harmonic vibrational frequencies. Unless otherwise noted, the values of 0.9806, 0.9989, and 1.0015 were employed in calculating ZPVE, H_{temp}, and S values, respectively (corresponding to 298 K in the last two cases). Geometrical parameters in the text refer to B3-LYP/6-31+G(d,p) values. Relative energies (ΔE) correspond to MPWB1K/6-311+G(3df,-2p) values at 0 K, incorporating zero-point vibrational energies (ZPVEs) derived from scaled B3-LYP/6-31+G(d,p) frequencies. Unless otherwise noted, relative enthalpies (ΔH), entropies (ΔS), and free energies (ΔG) correspond to 298 K values. Mulliken

TABLE 1: Gas-Phase Energy (kJ mol^{-1}), Enthalpy (kJ mol^{-1}), Entropy (J mol^{-1} K^{-1}), and Free-Energy (kJ mol^{-1}) Profiles for the Transfer Hydrogenation between Acridan (ACD) and α-Methylstyrene (AMS)

			intermediates				
	TS1 (R)	TS1 (U)	radical	ionic	TS2 (R)	TS2 (U)	products
ΔE^a	145.2	131.7	95.6	576.6	168.5	137.2	−33.7
ΔH^b	152.7	140.3	103.2	582.7	177.3	145.8	−31.3
ΔS^b	−110.2	−98.1	52.5	32.1	−99.7	−96.3	16.2
ΔG^b	215.9	196.6	73.1	564.4	234.5	200.9	−40.5

[a] 0 K values. [b] 573 K, which was the temperature employed in the experimental studies.[5] Scale factors of 0.9806 (ZPVE), 0.9816 (ΔH_{temp}), and 0.9910 (S) (corresponding to 573 K) were used.[17]

charges and spin densities[18] were obtained at the UB3-LYP/6-31+G(d,p) level.
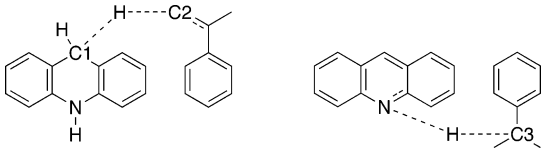
Free energies of solvation (ΔG_{solv}) were evaluated by using two polarizable continuum models (PCMs) of solvation, specifically the integral-equation-formalism PCM model (IEF-PCM)[19] and the conductor-like PCM model (C-PCM).[20] The choice of cavity used in such approaches can lead to vastly different free energies of solvation. We evaluated three different sets of cavities in the present study, namely, UA0, UAHF, and UAKS. The UA0 cavities are derived by using the united atom topological model (UATM),[21] using atomic radii from the universal force field (UFF).[22] The UAHF and UAKS cavities are obtained with UATM and radii optimized for free energies of solvation (in water) for a test set of molecules at the HF/6-31G(d) and PBE0/6-31G(d) levels. We find that the combination of B3-LYP/6-31+G(d,p), the IEF-PCM solvation model, and UA0 cavities gives free-energy barriers that are in best agreement with experiment (see below). Therefore, unless otherwise noted, free energies of solvation were obtained by using this combination of computational method, continuum model, and atomic radii.

Preliminary calculations indicate that optimizations incorporating continuum solvation yield geometries for equilibrium structures similar to those obtained in the gas phase. As a result, there are only small differences in the MPWB1K/6-311+G-(3df,2p) barriers (<2 kJ mol^{-1}) compared with those obtained with condensed-phase geometries. However, the geometries of some of the transition structures obtained in the presence of a continuum deviate significantly from the gas-phase structures, and this leads to larger differences in the high-level single-point barriers (~10 kJ mol^{-1}). In light of these findings, solvent effects for equilibrium structures have been evaluated with single-point-energy calculations on the gas-phase geometries, whereas solvent effects for transition structures, unless otherwise noted, have been obtained by using geometries optimized in the presence of a continuum.

3. Results and Discussion

3.1. Acridan (ACD)/α-Methylstyrene (AMS). The reaction between acridan and α-methylstyrene (eq 1) is mildly exothermic, with a free energy of reaction of −40.5 kJ mol^{-1} in the gas phase (Table 1). Optimization with UB3-LYP gives transition structures that are similar to those obtained with RB3-LYP. The UMPWB1K single-point calculations, however, lead to significantly lower relative energies (by up to 34 kJ mol^{-1}) than RMPWB1K.

The transition structures have considerable biradical character, as indicated by the $\langle S^2 \rangle$ values of 0.18 and 0.41, for the transition structures for the first (TS1) and second (TS2) steps, respectively. The energy, enthalpy, and free energy of the radical intermediates are substantially lower than those of the ionic

TABLE 2: Selected Interatomic Distances (Å) for the Transition Structures for Transfer Hydrogenation between Acridan and α-Methylstyrene, Optimized at the UB3-LYP/6-31+G(d,p) Level in Various Solvents

	TS1			TS2		
solvent[a]	C1···H	H···C2	C1···C2	N···H	H···C3	N···C3
gas phase	1.600	1.234	2.833	1.153	1.637	2.766
heptane	1.598	1.234	2.831	1.151	1.643	2.769
ether	1.596	1.234	2.830	1.148	1.650	2.774
acetone	1.595	1.234	2.829	1.147	1.653	2.776
CH$_3$CN	1.595	1.234	2.829	1.146	1.654	2.777

[a] The solvents are listed in ascending order of their dielectric constant (ϵ). The ϵ values for vacuum, heptane, ether, acetone, and acetonitrile (CH$_3$CN) are 1.0, 1.9, 4.3, 20.7, and 36.6, respectively.

intermediates. This, together with the biradical character of the transition structures, suggests that a radical mechanism is preferred over an ionic one, consistent with the conclusion reached previously on the basis of experimental observations.[5]

The calculated transition structures resemble the geometries for the intermediates more than those for the reactants, as indicated by the substantially shorter lengths for H···C2 (TS1) and N···H (TS2) (~1.2 Å) compared with those for C1···H and H···C3 (~1.6 Å), respectively (Table 2). For this reaction, the optimized transition structures are relatively insensitive to the solvent (variations <0.01 Å). Nonetheless, there is a slight trend for both transition structures to become earlier (shorter C1···H for TS1 and longer H···C3 for TS2) as the solvent becomes more polar. While these effects are very small, we point them out here because similar but more significant trends are observed for other reactions investigated (to be discussed below).

The condensed-phase free-energy profile calculated at the UMPWB1K/6-311+G(3df,2p) level (Table 3) is generally relatively insensitive to the methodology employed for the calculation of the free energy of solvation. For example, B3-LYP and HF give rise to relative energies that are generally within 5 kJ mol^{-1} of one another. One exception is TS2, for which the relative energies with RB3-LYP solvation are substantially higher than the corresponding RHF values (Table S4 of the Supporting Information). In addition, the C-PCM model leads to relative energies that are very similar (±1 kJ mol^{-1}) to the corresponding IEF-PCM values. On the other hand, while UAKS and UAHF cavities give very similar (±3 kJ mol^{-1}) relative energies, the use of UA0 atomic radii leads to significantly lower barriers and to lower relative energies for the ionic intermediates. The barriers obtained with UA0 cavities are in fact in better agreement with experiment (overestimated by up to 10 kJ mol^{-1}), than those employing UAKS and UAHF atomic radii (overestimated by up to 35 kJ mol^{-1}). It has been previously demonstrated that, while the C-PCM/UAKS methodology gives good agreement with experimental ΔG_{solv} and pK_a for molecules at their equilibrium geometry, it overestimates barriers by up to 40 kJ mol^{-1}.[23] Our observations for the C-PCM/UAKS model are consistent with these previous findings.[23] As a result of these comparisons, we have chosen the B3-LYP/6-31+G(d,p)/IEF-PCM/UA0 combination to obtain the condensed-phase free-energy profiles for the remaining reactions in this paper. For the ACD/AMS reaction, the use of gas-phase geometries for the transition structures leads to relative energies

Study of Uncatalyzed Transfer Hydrogenation

J. Phys. Chem. A, Vol. 111, No. 28, 2007 **6459**

TABLE 3: Condensed-Phase UMPWB1K/6-311+G(3df,2p) Free-Energy Profiles[a] (kJ mol^{-1}) for the Transfer-Hydrogenation Reaction between Acridan and α-Methylstyrene, with Free Energies of Solvation Obtained with Various Methodologies

solvent[b]	method[c]	continuum	cavity	TS1[d]	intermediates		TS2[d]	products
					radical	ionic		
acetone (20.7)	UB3-LYP	IEF-PCM	UAKS	214.1[e]	70.3	247.9	220.2[e]	−40.5
	UB3-LYP	IEF-PCM	UAKS	210.1	70.3	247.9	221.7	−40.5
	UB3-LYP	IEF-PCM	UAHF	210.3	70.5	249.3	219.8	−40.3
	UB3-LYP	IEF-PCM	UA0	187.9[e]	72.3	214.7	210.4[e]	−33.1
	UB3-LYP	IEF-PCM	UA0	188.4	72.3	214.7	212.2	−33.1
	UHF	IEF-PCM	UAKS	213.8	74.3	246.0	222.5	−40.9
	UHF	C−PCM	UAKS	214.1	74.4	245.2	222.9	−40.7
CH$_3$CN (36.6)	UB3-LYP	IEF-PCM	UAKS	210.7[e]	70.4	240.3	216.1[e]	−40.3
	UB3-LYP	IEF-PCM	UAKS	206.0	70.4	240.3	217.9	−40.3
	UB3-LYP	IEF-PCM	UAHF	206.2	70.6	241.8	215.7	−40.2
	UB3-LYP	IEF-PCM	UA0	179.7[e]	72.4	206.5	202.7[e]	−32.3
	UB3-LYP	IEF-PCM	UA0	180.2	72.4	206.5	204.4	−32.3
	UHF	IEF-PCM	UAKS	209.9	74.6	238.3	218.7	−40.7
	UHF	C−PCM	UAKS	210.0	74.7	237.8	218.9	−40.6
triglyme (7.2)	Expt			177.8				
pyridine (13.3)	Expt			178.2				
NMA[f] (179.0)	Expt			177.0				

[a] 573 K values. [b] Dielectric constants (ε) of the solvents are shown in parentheses. [c] The 6-31+G(d,p) basis set was used in the calculation of ΔG_{solv}. [d] Condensed-phase geometries were used unless noted otherwise. [e] Gas-phase geometries. [f] *N*-Methylacetamide.

TABLE 4: Free-Energy Profiles (kJ mol^{-1}) for the Transfer-Hydrogenation Reaction between Acridan and α-Methylstyrene in Various Solvents

solvent	TS1[a]	intermediates		TS2[a]	products
		radical	ionic		
gas phase	196.6	73.1	564.4	200.9	−40.5
heptane	190.1	73.6	393.1	202.7	−36.8
ether	185.3	73.1	285.7	204.0	−34.8
acetone	188.4	72.3	214.7	212.2	−33.1
CH$_3$CN	180.2	72.4	206.5	204.4	−32.3

[a] Geometries of the condensed-phase transition structures were optimized in the presence of their respective solvent continuum.

similar to those obtained with condensed-phase geometries (±5 kJ mol^{-1}). This is consistent with the similarity in the gas-phase and condensed-phase transition structures (Table 2) but this observation does not hold for some of the other reactions examined.

The free-energy profile for the reaction between acridan and α-methylstyrene is relatively insensitive to the solvent, with the exception of the relative energies for the ionic intermediates, which decrease dramatically as the polarity of the solvent increases (Table 4). Among the four solvents studied, the barriers for both steps lie within a range of 10 kJ mol^{-1}. This is consistent with the experimental observation that the rate of reaction is rather independent of the solvent.[1a] The barrier for the first step generally decreases with increasing polarity of the solvent. This is consistent with an earlier transition structure in a more polar solvent, as discussed above (Table 2) and in accord with the Hammond postulate.[24] On the other hand, there is no obvious trend in the barrier for the second step. While the relative energy of the ionic intermediates decreases considerably as the solvent becomes more polar, it remains substantially higher (by more than 130 kJ mol^{-1}) than that of the radical intermediates, even in the most polar solvent examined. Thus, the radical pathway appears to be favored in all solvents examined. This is supported by the ⟨S^2⟩ values of 0.18, 0.17, 0.17, and 0.17 for TS1 in heptane, ether, acetone, and CH$_3$CN, respectively, and the respective ⟨S^2⟩ values for TS2 of 0.39, 0.38, 0.39, and 0.34.

To further elucidate the nature of the reaction in various solvents, structures that lead from TS1 to the intermediates were obtained from IRC calculations. The Mulliken spin and charge

densities for the β-hydrogenated-α-methylstyrene fragments of these structures along the reaction coordinate are shown in Figure 2. Both spin and charge densities can be seen to be rather insensitive to the solvent along the entire reaction coordinate examined. This is in accord with the previous observations that the geometries (Table 2) and relative energies (Table 4) also have little dependence on the solvent. While the charge densities remain close to zero along the reaction coordinate in all solvents examined, the spin densities increase gradually as the structures approach those of the intermediates. This further strengthens the proposition of a radical mechanism.

3.2. 1,4-Cyclohexadiene (CHD)/2,3-Dichloro-5,6-dicyano-1,4-benzoquinone (DDQ). For the reaction between 1,4-cyclohexadiene (CHD) and 2,3-dichloro-5,6-dicyano-1,4-benzoquinone (DDQ) (eq 2), we were unable to locate a transition structure for the second step involving hydrogen atom/proton transfer between the intermediates to form the final products (i.e., analogous to TS2 in the ACD/AMS reactions) despite numerous attempts. Preliminary rigid scans (Figure 3) indicate that this process is likely to be barrier-free at the B3-LYP, MPWB1K, HF, and MP2 levels of theory with the 6-31+G-(d,p) basis set. Similarly, for the CHD/PBQ (section 3.4) and DHP/PBQ (section 3.5) reactions, we have not been able to locate a transition structure for the reaction between the intermediates to form the product. Presumably this is associated with the high exothermicity of this step in the CHD/DDQ (Table 5), CHD/DDQ (Table 9) and DHP/PBQ (Table 11) reactions. For the gas-phase reaction between 1,4-cyclohexadiene and DDQ, we find that the ionic intermediates have significantly higher energies than the radical intermediates, indicative of a radical pathway.

Selected interatomic distances for TS1 in the transfer hydrogenation between 1,4-cyclohexadiene (CHD) and DDQ, optimized at the UB3-LYP/6-31+G(d,p) level in various solvents, are displayed in Table 6. We can see that, as the polarity of the solvent increases, the transition structure for the transfer-hydrogenation reaction between 1,4-cyclohexadiene and DDQ becomes earlier, i.e., more reactant-like (shorter C···H and longer H···O).

Results for the condensed-phase (heptane and ether) free-energy profile of transfer hydrogenation between 1,4-cyclo-hexadiene with DDQ (Table 7) show that the use of UAKS
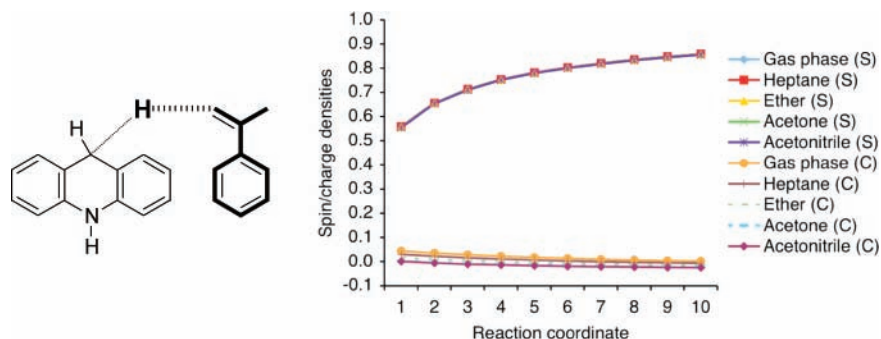
Figure 2. UB3-LYP/6-31+G(d,p) spin (S) and charge (C) densities for the β-hydrogenated-α-methylstyrene moiety in TS1 (**1**) and subsequent structures (**2−10**) along the IRC in the direction of the intermediates, for the reaction between acridan and α-methylstyrene in various solvents.
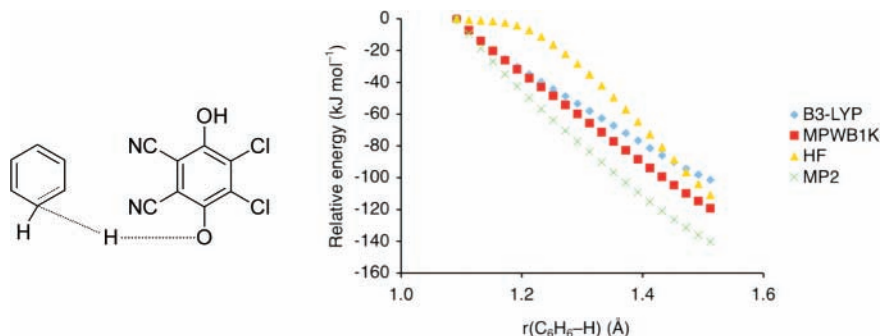

Figure 3. Gas-phase rigid scans ($r(C_6H_6-H)$) for hydrogen transfer between the intermediates ($C_6H_7^{\bullet}$ and DDQH$^{\bullet}$) in the transfer-hydrogenation reaction of 1,4-cyclohexadiene with DDQ. The 6-31+G(d,p) basis set was employed throughout.

TABLE 5: Free-Energy Profiles (kJ mol^{-1}) for the Transfer-Hydrogenation Reaction between 1,4-Cyclohexadiene (CHD) and DDQ in Various Solvents

		intermediates		
solvent	TS1	radical	ionic	products
gas phase	92.2	16.3	321.1	−247.6
heptane	94.8	8.8	133.3	−255.1
ether	90.1	3.0	20.4	−259.4
acetone	91.2	−1.7	−49.9	−262.5
CH$_3$CN	85.8	−2.7	−58.2	−263.7

TABLE 6: Selected Interatomic Distances (Å) for TS1 in the Transfer Hydrogenation between 1,4-Cyclohexadiene and DDQ, Optimized at the UB3-LYP/6-31+G(d,p) Level in Various Solvents

	C···H	H···O	C···O
gas phase	1.377	1.207	2.567
heptane	1.352	1.232	2.566
ether	1.319	1.272	2.570
acetone	1.308	1.288	2.573
CH$_3$CN	1.305	1.291	2.574

TABLE 7: Condensed-Phase Free-Energy Profiles (kJ mol^{-1}) for the Transfer-Hydrogenation Reaction between 1,4-Cyclohexadiene and DDQ, with Free Energies of Solvation Obtained with Various Methodologies[a]

			intermediates		
solvent[b]	cavity	TS1[c]	radical	ionic	products
heptane (1.9)	UAKS	103.9[d]	12.6	146.6	−247.8
	UAKS	107.4	12.6	146.6	−247.8
	UA0	91.2[d]	8.8	133.3	−255.1
	UA0	94.8	8.8	133.3	−255.1
ether (4.3)	UAKS	95.8[d]	9.1	26.5	−242.9
	UAKS	103.0	9.1	26.5	−242.9
	UA0	82.5[d]	3.0	20.4	−259.4
	UA0	90.1	3.0	20.4	−259.4
dioxane (2.2)	Expt	84.1			

[a] The B3-LYP/6-31+G(d,p) method and the IEF-PCM continuum model were employed. [b] Dielectric constants (ϵ) of the solvents are shown in parentheses. [c] Condensed-phase geometries were used unless noted otherwise. [d] Gas-phase geometries.

obtained from condensed-phase geometries (up to 8 kJ mol^{-1}). This is consistent with the fact that the condensed-phase optimized geometries differ significantly from the gas-phase geometries for this reaction (variations of up to ∼0.1 Å, Table 6).

For the transfer-hydrogenation reaction between 1,4-cyclohexadiene and DDQ in various solvents (Table 5), the barrier varies within a narrow range of 10 kJ mol^{-1}, with a slight trend of decreasing barrier with increasing solvent polarity. This suggests that there is a relatively small extent of charge separation at this stage of the reaction. The overall reaction becomes more exothermic as the polarity of the solvent increases. We observe similar effects of solvent on the overall exothermicity for the CHD/PBQ (Table 9) and DHP/PBQ (Table 11) reactions. This is presumably due to the presence of the more polar OH moiety in the hydroquinone products in these reactions, as opposed to the less polar C=O group in the quinone reactants.
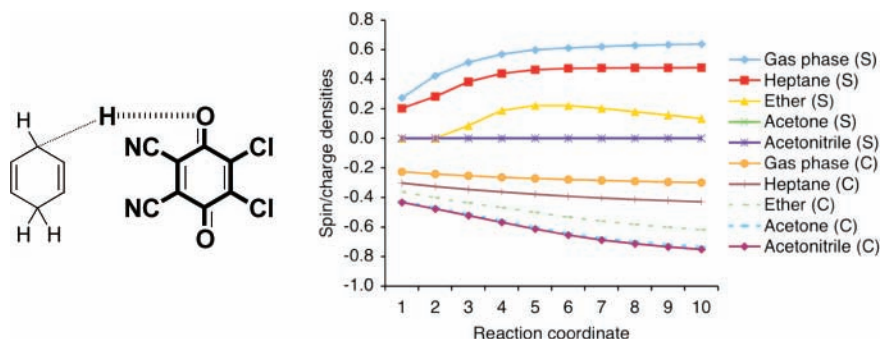
cavities leads to higher relative energies than with UA0 atomic radii. The differences between the UAKS and UA0 values are more noticeable for the ionic intermediates and the transition structure (up to 13 kJ mol^{-1}). For the CHD/DDQ reaction (Table 7), the UA0 cavities give barriers that are more consistent with the experimental values, as also observed above for the ACD/AMS reaction. These results further reinforce our choice of the B3-LYP/6-31+G(d,p)/IEF-PCM/UA0 model for the calculation of free energies of solvation. The use of gas-phase geometries leads to substantial differences in barriers compared with those

Study of Uncatalyzed Transfer Hydrogenation

J. Phys. Chem. A, Vol. 111, No. 28, 2007 **6461**

Figure 4. UB3-LYP/6-31+G(d,p) spin (S) and charge (C) densities for the O-hydrogenated-DDQ moiety in TS1 (**1**) and subsequent structures (**2**−**10**) along the IRC in the direction of the intermediates, for the reaction between 1,4-cyclohexadiene and DDQ in various solvents.

There is little variation with solvent in the relative energies for the radical intermediates but a large variation for the ionic intermediates (Table 5). Intriguingly, for the CHD/DDQ reaction the radical intermediates are substantially lower in energy (by more than 120 kJ mol^{-1}) only in the gas phase and in heptane. For the reaction in ether, the radical and ionic intermediates have similar energies (within 20 kJ mol^{-1}), while in acetone and CH$_3$CN the ionic intermediates are markedly lower in energy (by more than 40 kJ mol^{-1}). These results indicate that for the CHD/DDQ reaction in heptane, a radical mechanism is favored. This is consistent with the radical mechanism proposed on the basis of experimental observations, as the dielectric constant of heptane (1.9) is close to that (2.2) of the dioxane solvent used experimentally. However, in more polar solvents, namely, acetone and CH$_3$CN, the ionic mechanism is more likely to be the dominant pathway, while in ether both pathways may be operative. Thus, a change in the mechanism with the solvent appears likely for this reaction. This proposition is supported by the $\langle S^2 \rangle$ values for the transition structure for the reactions, which decrease dramatically as the solvent becomes more polar. Thus, the $\langle S^2 \rangle$ values for TS1 optimized in the gas phase, heptane, ether, acetone, and CH$_3$CN are 0.11, 0.06, 0.00, 0.00, and 0.00, respectively. In the last three cases, numerous attempts at optimizing unrestricted transition structures led to restricted solutions with zero $\langle S^2 \rangle$ values.

To further elucidate the potential of a change in mechanism with respect to the solvent, various structures starting from TS1 and moving in the direction of the intermediates were obtained from IRC calculations. The total spin and charge densities of the O-hydrogenated-DDQ fragment (DDQH) of these structures are plotted against the reaction coordinate in Figure 4. The DDQH moiety in the reaction profile has significant negative charge along the reaction coordinate in all solvents. This indicates the ionic nature of the CHD/DDQ reaction, and is presumably due to the ability of the electron-withdrawing chloro and cyano groups on DDQ to stabilize the DDQH$^-$ ion.

Both the spin and charge densities along the reaction coordinate are substantially influenced by the solvent. For the reactions in the two least polar media, namely, the gas phase and heptane, the spin densities increase steadily from about 0.2 to a plateau of approximately 0.6 and 0.4 respectively for the gas-phase reaction and the reaction in heptane. On the other hand, the charge densities both in the gas phase and in heptane become more negative at a slower pace compared with the corresponding changes in spin densities, and remain in a narrower range of 0.1. These variations in the spin and charge densities are more consistent with a mechanism that involves intermediate radicals than ions, and are in accord with the relative energies of the radical and ionic intermediates (Table 5).

For the reaction in ether, the spin density increases initially from zero to a maximum of about 0.2 before steadily declining.
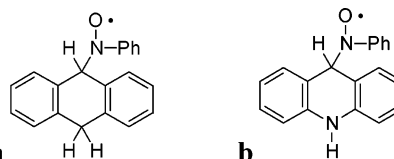

Figure 5. Radical adduct (**a**) identified in the reaction between 9,10-dihydroanthracene and DDQ in the presence of nitrosobenzene, and a possible adduct (**b**) in the reaction between acridan and DDQ in the presence of nitrosobenzene.
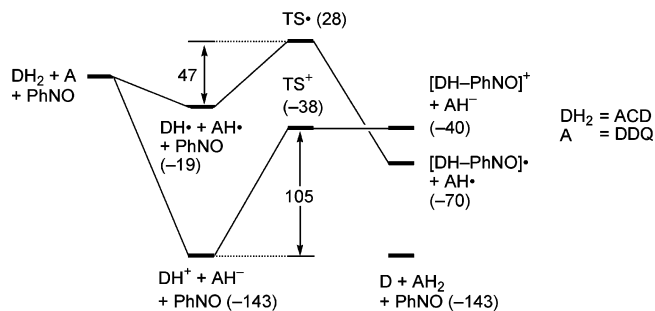

Figure 6. Free-energy profile (energies in kJ mol^{-1} shown in parentheses) for the transfer-hydrogenation reaction between the donor acridan (denoted DH$_2$) and the acceptor DDQ (denoted A) in acetonitrile, in the presence of nitrosobenzene (PhNO).

The corresponding charge density becomes more negative, moving from −0.4 to −0.6 as the reaction progresses. An intriguing feature of the CHD/DDQ reaction is that with the most polar solvents, namely, acetone and CH$_3$CN, there is zero spin density along the entire reaction coordinate. Numerous attempts at locating unrestricted solutions for these structures in acetone or CH$_3$CN all led to restricted solutions. The corresponding charge density becomes more negative, changing from −0.4 in the transition structure to −0.8. These observations suggest an ionic rather than a radical mechanism, which is consistent with the lower energy of the ionic intermediates relative to the radical intermediates (Table 5). Thus, the variations in the spin- and charge-density profiles in various solvents point toward a change in reaction mechanism with solvent polarity, in a similar manner to that suggested by the variation in relative energies between the radical and ionic intermediates.

3.3. 9,10-Dihydroanthracene (DHA)/DDQ and Acridan (ACD)/DDQ. 9,10-Dihydroanthracene (DHA) has been observed to react with DDQ in dioxane ($\epsilon = 2.2$) to give anthracene quantitatively.[25] A spin-trapping experiment with nitrosobenzene yielded the EPR spectrum of the radical-adduct **a** shown in Figure 5. Similarly, in the reaction between acridan and DDQ in acetonitrile, with nitrosobenzene as the spin-trap, a well-resolved EPR spectrum was obtained,[1a,25] which is likely to be associated with a similar radical adduct (adduct **b** in Figure
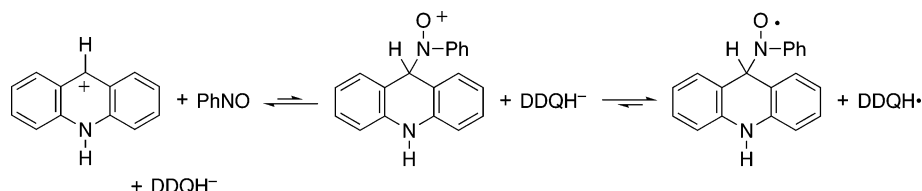
Figure 7. A possible pathway for the formation of the radical adduct between monohydroacridine and nitrosobenzene from the initially formed ion pair in the reaction between acridan and DDQ in acetonitrile.
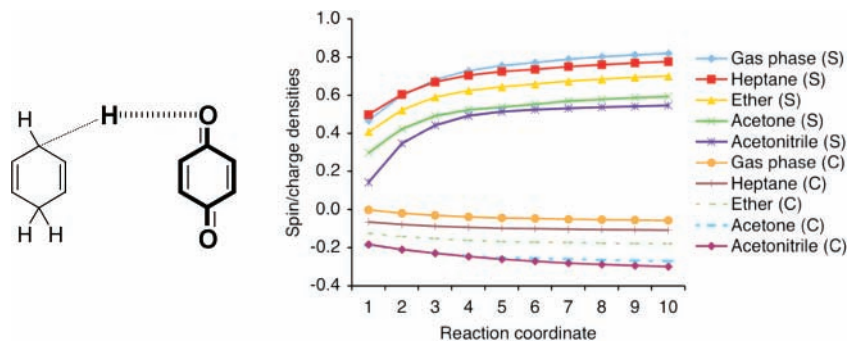

Figure 8. UB3-LYP/6-31+G(d,p) spin (S) and charge (C) densities for the O-hydrogenated-quinone moiety in TS1 (**1**) and subsequent structures (**2**−**10**) along the IRC in the direction of the intermediates, for the reaction between 1,4-cyclohexadiene and *p*-benzoquinone in various solvents.

5). These results indicate the presence of radicals under the conditions employed in these two reactions, and thus argue in favor of radical over ionic mechanisms.

The overall reaction of 9,10-dihydroanthracene with DDQ (eq 3, Table 8) is highly exothermic. In addition, the relative energies for the radical and ionic intermediates suggest a change in mechanism from radical to ionic as the solvent becomes more polar. Our finding that, in a relatively nonpolar solvent such as heptane (ϵ = 1.9), the radical mechanism is likely to be the dominant pathway is consistent with the experimental observation of radicals in spin-trapping experiments in dioxane (ϵ = 2.2).[25] However, we predict that this is less likely to be the case in more polar solvents.

For the reaction of acridan with DDQ (eq 4, Table 8), the radical intermediates are again lower in energy than the ionic intermediates in the gas phase and in heptane. On the other hand, for the reactions in ether, acetone, and CH₃CN, the ionic intermediates are substantially lower in energy than the radical intermediates. This is in apparent contradiction to experiment, in which spin-trapping with nitrosobenzene indicates the presence of radicals in the reaction of acridan with DDQ in acetonitrile.[1a,25] To explore for possible reasons behind the apparent discrepancy between our calculated results and the experimental observations, we investigated the reactions between the 9-monohydroacridine intermediates, both radical and cationic, with the spin-trapping agent nitrosobenzene. The relative free energies for the species involved in the transfer-hydrogenation reaction in the presence of PhNO in acetonitrile are shown in Figure 6, in which the donor acridan is denoted DH₂ while the acceptor DDQ is denoted A.

There is a modest barrier (47 kJ mol⁻¹) to the formation of the adduct between monohydroacridine radical and nitrosobenzene [DH-PhNO]•. On the other hand, due to less favorable thermodynamics (ΔG = +103 kJ mol⁻¹), the barrier for the combination of monohydroacridine cation with nitrosobenzene to give the ionic adduct [DH-PhNO]⁺ is considerably higher (105 kJ mol⁻¹). A striking feature of the free-energy profile is that, although the initial ion pair (DH⁺ + AH⁻) has a lower energy than the radical pair (DH• + AH•), the ion pair involving the adduct with nitrosobenzene ([DH-PhNO]⁺ + AH⁻) lies higher in energy than the corresponding radical pair ([DH-

TABLE 8: Free-Energy Profiles (kJ mol⁻¹) for the Transfer-Hydrogenation Reaction between Donors 9,10-Dihydroanthracene (DHA) and Acridan (ACD) with the Acceptor DDQ in Various Solvents

	9,10-dihydroanthracene			acridan		
	intermediates			intermediates		
solvent	radical	ionic	products	radical	ionic	products
gas phase	18.0	278.4	−159.3	1.9	196.4	−138.1
heptane	10.8	114.8	−166.2	−6.1	29.2	−141.7
ether	5.4	16.4	−170.0	−12.3	−71.9	−142.7
acetone	0.7	−44.8	−173.1	−17.5	−135.7	−142.8
CH₃CN	−0.2	−52.0	−174.0	−18.5	−143.2	−143.1

PhNO]• + AH•). Presumably, the lower energy of the radical-adduct pair leads to its eventual formation, and hence this may account for the signals detected in EPR experiments.

A possible pathway from the initially formed ion pair is illustrated in Figure 7. In this pathway, the monohydroacridine cation is first trapped by nitrosobenzene, following which electron transfer from the DDQH⁻ anion to the cationic adduct gives the final radical pair. The first step is an endothermic process, with a barrier of 105 kJ mol⁻¹ (Figure 6), while the electron-transfer step is exothermic by 30 kJ mol⁻¹. Therefore, trapping of the cationic intermediate by nitrosobenzene is likely to be the rate-limiting step in the generation of the radical adduct. Presumably, the highly exothermic hydride-transfer reaction from acridan to DDQ that precedes the trapping reaction (Figure 6) partially supplies the energy required to overcome the barrier. Alternatively, a small amount of the radical pair could be produced from the reactants, and the subsequent trapping of monohydroacridine radical by nitrosobenzene may also contribute to the formation of the radical adduct.

3.4. 1,4-Cyclohexadiene (CHD)/*p*-Benzoquinone (PBQ). For the transfer-hydrogenation reaction between 1,4-cyclohexadiene (CHD) and *p*-benzoquinone (PBQ) (eq 5), the barriers in various solvents span a narrow range of 13 kJ mol⁻¹, with a more polar solvent giving a lower barrier than a less polar solvent. The energy of the radical intermediates also decreases from 36.3 kJ mol⁻¹ to 16.1 kJ mol⁻¹ as the polarity of the solvent increases. There is a more dramatic decrease in the energies of the ionic intermediates as the solvent becomes more polar, with the energy dropping by 237 kJ mol⁻¹. Despite the
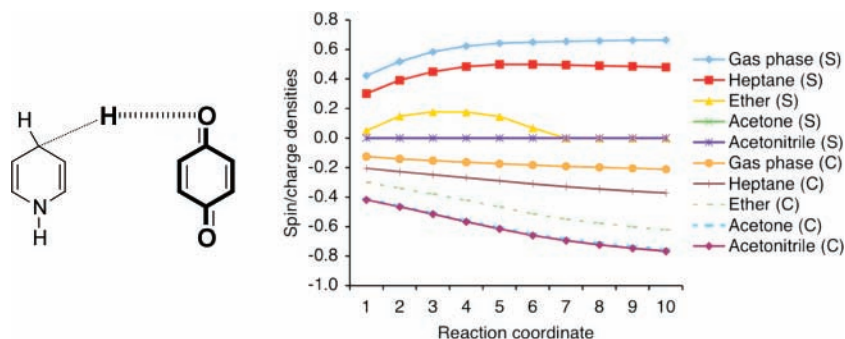
Study of Uncatalyzed Transfer Hydrogenation

J. Phys. Chem. A, Vol. 111, No. 28, 2007 **6463**

Figure 9. UB3-LYP/6-31+G(d,p) spin (S) and charge (C) densities for the O-hydrogenated-quinone moiety in TS1 (**1**) and subsequent structures (**2**−**10**) along the IRC in the direction of the intermediates, for the reaction between 1,4-dihydropyridine and *p*-benzoquinone in various solvents.
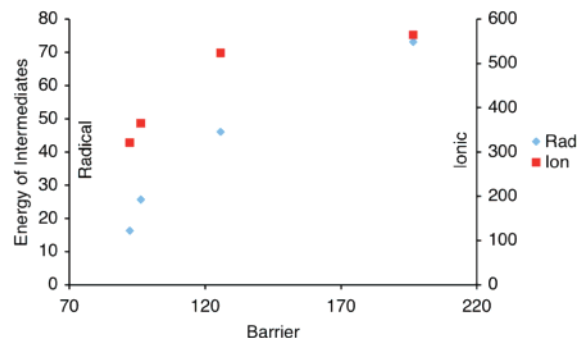

Figure 10. Gas-phase free-energy barriers for the initial hydrogen transfer (0 K, kJ mol^{-1}) versus free energies of the intermediates (0 K, kJ mol^{-1}) for reactions 1, 2, 5, and 6.
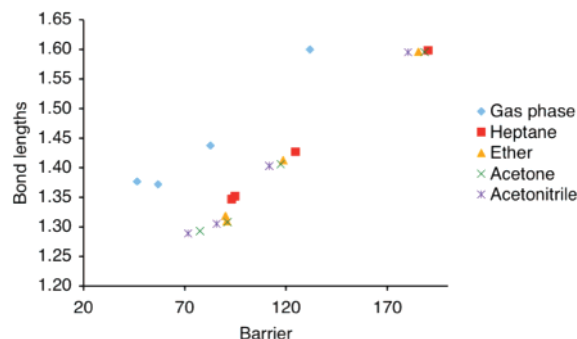
Figure 11. The breaking X_D···H distances (Å) in the transition structures for the hydrogen transfer X_D−H + Y_A → $X_D^\bullet$ + H−$Y_A^\bullet$ in reactions 1, 2, 5, and 6 plotted against the reaction barrier (kJ mol^{-1}).
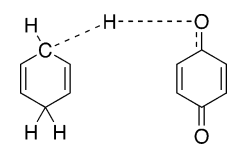
TABLE 9: Free-Energy Profiles (kJ mol^{-1}) for the Transfer-Hydrogenation Reaction between 1,4-Cyclohexadiene and *p*-Benzoquinone in Various Solvents

| solvent | TS1 | intermediates | | products |
		radical	ionic	
gas phase	125.6	46.1	523.8	−195.9
heptane	124.6	36.3	308.4	−206.8
ether	118.5	26.8	172.5	−216.7
acetone	117.3	17.6	82.2	−226.8
CH$_3$CN	111.7	16.1	71.2	−228.6

substantial lowering of the energy of the ionic intermediates with polar solvents such as acetone and CH$_3$CN, their energy remains higher than that for the radical intermediates by more than 50 kJ mol^{-1}. Thus, the relative energies of the radical and ionic intermediates seem to indicate a predominantly radical mechanism in all solvents investigated.

For the CHD/PBQ reaction, the transition structure becomes more reactant-like as the polarity of the solvent increases (Table 10). Thus, the C···H bond of cyclohexadiene that is involved in the transfer hydrogenation becomes shorter, while the H···O

TABLE 10: Selected Interatomic Distances (Å) for TS1 in the Transfer Hydrogenation between 1,4-Cyclohexadiene and *p*-Benzoquinone, Optimized at the UB3-LYP/6-31+G(d,p) Level in Various Solvents

	C···H	H···O	C···O
gas phase	1.438	1.155	2.580
heptane	1.427	1.163	2.575
ether	1.413	1.175	2.570
acetone	1.406	1.180	2.567
CH$_3$CN	1.403	1.182	2.567

distance in the monohydroquinone moiety becomes longer. For this reaction, the magnitude of the variation in bond distances is ∼0.03−0.04 Å. The $\langle S^2 \rangle$ values for the transition structure optimized in heptane, ether, acetone, and CH$_3$CN are 0.15, 0.05, 0.00, and 0.00, respectively. The trend in these $\langle S^2 \rangle$ values points toward a possible change in mechanism from radical to ionic as the solvent becomes more polar. This is in contrast to what would be expected from the relative energies of the radical and ionic intermediates, which suggest a radical pathway for the reaction in all solvents examined.

To clarify the mechanism of the reaction in various solvents, the spin and charge densities of the O-hydrogenated-*p*-benzo-quinone moiety (PBQH) in the structures along the IRC were analyzed (Figure 8). The spin and charge densities of the PBQH fragment show a significant sensitivity to solvent. With a more polar solvent, the spin density is lower and the charge is more negative. As the reaction progresses, the spin density increases rapidly in all solvents, and the charge on the PBQH moiety becomes more negative. The change in the charge density on the PBQH fragment is relatively independent of the solvent, with the PBQH moiety in the final IRC structure being ∼0.1 more negative than that in the TS.
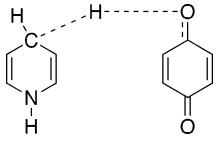
When the trends in the spin density are compared with those in the charge density, it is evident that as the reaction progresses, the PBQH moiety develops more radical character than ionic character, regardless of the solvent. This is suggestive of a radical mechanism for the transfer-hydrogenation reaction in all solvents investigated, and is consistent with the lower energies for the radical intermediates compared with those for the ionic intermediates (Table 9). The zero or very low $\langle S^2 \rangle$ values for the TS in the more polar solvents appear to indicate a relatively small extent of development of radical character in the C$_6$H$_7^\bullet$ and PBQH$^\bullet$ fragments at this stage of the reaction.

3.5. 1,4-Dihydropyridine (DHP)/*p*-Benzoquinone (PBQ). For the reaction between 1,4-dihydropyridine (DHP) and

TABLE 11: Free-Energy Profiles (kJ mol⁻¹) for the Transfer-Hydrogenation Reaction between 1,4-Dihydropyridine and *p*-Benzoquinone in Various Solvents

solvent	TS1	intermediates		products
		radical	ionic	
gas phase	96.3	25.7	365.0	−175.4
heptane	93.2	15.0	145.4	−182.5
ether	90.8	4.8	6.7	−189.9
acetone	77.5	−5.2	−85.4	−197.8
CH₃CN	71.6	−6.8	−96.6	−199.1

TABLE 12: Selected Interatomic Distances (Å) for TS1 for the Transfer Hydrogenation between 1,4-Dihydropyridine and *p*-Benzoquinone, Optimized at the UB3-LYP/6-31+G(d,p) Level in Various Solvents

	C···H	H···O	C···O
gas phase	1.372	1.203	2.558
heptane	1.347	1.224	2.554
ether	1.310	1.266	2.554
acetone	1.293	1.289	2.559
CH₃CN	1.289	1.295	2.560

p-benzoquinone (PBQ) (eq 6), the barriers for the initial hydrogen transfer to form the intermediates decrease as the solvent becomes more polar. The range in the barriers is ∼25 kJ mol⁻¹. The energies of the intermediates also decrease as the polarity of the solvent increases. For the radical intermediates, the energy spans a range of 33 kJ mol⁻¹, while for the ionic intermediates there is a much wider range of 241 kJ mol⁻¹.

In the gas phase, the energy of the ionic intermediates is much higher than that for the radical intermediates, and this is indicative of a radical mechanism. In condensed phases, the energies of the ionic intermediates remain higher than those for the radical intermediates only in heptane, while for ether the energies of the two types of intermediates are comparable, and in acetone and CH₃CN the energies for the ionic intermediates are substantially lower. This suggests a change in mechanism from radical to ionic as the polarity of the solvent increases. $\langle S^2 \rangle$ values for the transition structures in the gas phase, heptane, ether, acetone, and CH₃CN are 0.19, 0.13, 0.05, 0.00, and 0.00, respectively. This also supports a change in mechanism as the solvent becomes more polar. In the transition structures for the DHP/PBQ reaction, the C···H distance decreases and the H···O distance increases as the polarity of the solvent increases (Table 12), i.e., the transition structure becomes earlier as the solvent becomes more polar. For this reaction, the C···H and H···O distances span wide ranges of nearly 0.1 Å.

The Mulliken spin and charge densities for the monohydroquinone moiety in the structures along the IRC (from TS1 toward the intermediates) were examined in order to further elucidate the nature of the reaction in various solvents. Figure 9 shows that in the gas phase, the spin density of the monohydroquinone fragment increases steadily along the reaction coordinate, while the charge becomes more negative. However, the change in spin density is more prominent than the change in charge density, which supports a radical over an ionic mechanism. Similar trends in spin and charge densities are observed for the reaction in heptane. However, in this case the magnitudes of the changes for the two quantities are

TABLE 13: Free-Energy Profiles (kJ mol⁻¹) for Gas-Phase Transfer-Hydrogenation Reactions 1 (ACD/AMS), 2 (CHD/DDQ), 5 (CHD/PBQ), and 6 (DHP/PBQ)

reaction	TS1	intermediates		products	$E_I - E_R$
		radical	ionic		
1[a]	196.6	73.1	564.4	−40.5	+491.3
2[b]	92.2	16.3	321.1	−247.6	+304.8
5[b]	125.6	46.1	523.8	−195.9	+477.7
6[b]	96.3	25.7	365.0	−175.4	+339.3

[a] 573 K values. [b] 298 K values.

TABLE 14: Free-Energy Barriers (kJ mol⁻¹) and Donor−Hydrogen Distances (X_D···H, Å) in TS1 for Reactions 1, 2, 5, and 6 in Various Solvents[a]

	barrier				$X_D···H$ (TS1)[b]			
	(1)	(2)	(5)	(6)	(1)	(2)	(5)	(6)
gas phase	196.6	92.2	125.6	96.3	1.600	1.377	1.438	1.372
heptane	190.1	94.8	124.6	93.2	1.598	1.352	1.427	1.347
ether	185.3	90.1	118.5	90.8	1.596	1.319	1.413	1.310
acetone	188.4	91.2	117.3	77.5	1.595	1.308	1.406	1.293
CH₃CN	180.2	85.8	111.7	71.6	1.595	1.305	1.403	1.289

[a] Reaction 1 = ACD/AMS, reaction 2 = CHD/DDQ, reaction 5 = CHD/PBQ, and reaction 6 = DHP/PBQ. [b] $X_D···H$ = C1···H in Table 2 for reaction 1, while $X_D···H$ = C···H in Table 6 for reaction 2, in Table 10 for reaction 5, and in Table 11 for reaction 6.

comparable, and it is therefore not clear from these trends whether a radical or an ionic pathway is favored. This is in contrast to the relative energies for the radical and ionic intermediates (Table 11), which clearly favor a radical mechanism.

The trends for the reaction in ether represent a particularly interesting case. The spin density increases initially but subsequently decreases to zero, while the charge gradually becomes more negative in a monotonic manner. Thus, in ether it is likely that an ionic pathway is the more prominent mechanism compared with a radical pathway. With acetone and CH₃CN as the solvent, the spin density remains zero over the entire reaction coordinate examined, while the charge becomes more negative, from −0.40 at the transition structure to −0.80 at the last point of the IRC. This supports an ionic mechanism in these polar solvents, and is consistent with the energies for the ionic intermediates being much lower than those for the radical intermediates in these solvents (Table 11). Although the observed trends in spin and charge densities do not lead to a consistent conclusion about the mechanism for the reaction in some solvents, a comparison of these trends for a variety of solvents points toward a change in mechanism with solvent polarity. This is in accord with the trends in the relative energies for the two types of intermediates (Table 11).

3.6. Comparison of Reactions 1, 2, 5, and 6. The gas-phase free-energy profiles for reactions 1 (ACD/AMS), 2 (CHD/DDQ), 5 (CHD/PBQ), and 6 (DHP/PBQ) are shown in Table 13, while Figure 10 shows a plot of the barrier (at TS1) versus the energies of the intermediates, both radical and ionic, for these four reactions. The correlation between the barrier and the energies of the radical intermediates (via which all four reactions are indicated to proceed in the gas phase) has an R^2 value of 0.95.[26] Thus, it seems that, for the initial hydrogen atom-transfer step for these transfer-hydrogenation reactions, the Bell−Evans−Polanyi principle[27] holds reasonably well.

Table 14 shows the barriers for the four reactions in various solvents, together with the distance between the donor atom (X_D) and the hydrogen being transferred in TS1 for each reaction. For all four reactions, the barrier decreases and the

TABLE 15: $\langle S^2 \rangle$ Values and the Relative Energies of the Radical and Ionic Intermediates ($E_R - E_I$, kJ mol^{-1}) for Reactions 1, 2, 5, and 6 in Various Solvents^a

	$\langle S^2 \rangle$				$E_I - E_R$			
	(1)	(2)	(5)	(6)	(1)	(2)	(5)	(6)
gas phase	0.18	0.11	0.20	0.19	+491.3	+304.8	+477.7	+339.3
heptane	0.18	0.06	0.15	0.13	+319.5	+124.5	+272.1	+130.4
ether	0.17	0.00	0.05	0.05	+212.6	+17.4	+145.7	+1.9
acetone	0.17	0.00	0.00	0.00	+142.4	−48.2	+64.6	−80.2
CH$_3$CN	0.17	0.00	0.00	0.00	+134.1	−55.5	+55.1	−89.8

^{a} Reaction 1 = ACD/AMS, reaction 2 = CHD/DDQ, reaction 5 = CHD/PBQ, and reaction 6 = DHP/PBQ.

TABLE 16: Free-Energy Barriers (kJ mol^{-1}) and Proposed Mechanisms^a for Reactions 1, 2, 5, and 6 in Various Solvents^b

	barrier				mechanism^c			
	(1)	(2)	(5)	(6)	(1)	(2)	(5)	(6)
gas phase	196.6	92.2	125.6	96.3	R	R	R	R
heptane	190.1	94.8	124.6	93.2	R	R	R	R/I
ether	185.3	90.1	118.5	90.8	R	R/I	R	R/I
acetone	188.4	91.2	117.3	77.5	R	I	R	I
CH$_3$CN	180.2	85.8	111.7	71.6	R	I	R	I
range^d	16.4	9.0	13.9	24.7				

^{a} Based on the relative energies of the radical and ionic intermediate (Tables 4, 5, 8, and 9) and the spin and charge densities (Figures 2, 4, 8, and 9). ^{b} Reaction 1 = ACD/AMS, reaction 2 = CHD/DDQ, reaction 5 = CHD/PBQ, and reaction 6 = DHP/PBQ. ^{c} R = radical, I = ionic. ^{d} Range = maximum barrier − minimum barrier.

$X_D \cdots H$ distance becomes shorter as the polarity of the solvent increases. Thus, the transition structure becomes earlier as the barrier decreases. This is consistent with the Hammond postulate. The correlation between the barrier and the $X_D \cdots H$ distance holds remarkably well for a variety of reactions in a variety of solvents, as indicated in Figure 11 with a plot of the $X_D \cdots H$ distances in TS1 versus the reaction barriers. A separate $X_D \cdots H$/barrier correlation is observed for the gas-phase reactions.

The $\langle S^2 \rangle$ values for TS1 of reactions 1, 2, 5, and 6 in various solvents, and the respective energy differences between the radical and ionic intermediates ($E_I - E_R$), are shown in Table 15. A positive $E_I - E_R$ indicates that the radical intermediates lie lower in energy, and vise versa. The $\langle S^2 \rangle$ values for TS1 suggest a radical mechanism for all solvents for reaction 1, and a change of mechanism from radical to ionic for reactions 2, 5, and 6. For reactions 1, 2, and 6, the $E_I - R_R$ values in the various solvents are consistent with the corresponding $\langle S^2 \rangle$ values, but this is not the case for reaction 5. Based on the trends in charge and spin densities along the reaction coordinate (Figure 8), we proposed earlier that radical character might be developed at a stage of the reaction later than the transition structure.

Reaction 5 (CHD/PBQ) is related both to reaction 2 (CHD/DDQ) (same hydrogen atom donor) and reaction 6 (DHP/PBQ) (same hydrogen atom acceptor). The results in Table 15 show that the ionic intermediates are favored relative to the radical intermediates for the CHD/DDQ and DHP/PBQ reactions to a greater extent than for the CHD/PBQ reaction by more than 100 kJ mol^{-1}. For the CHD/DDQ reaction, this can be attributed to the presence of electron-withdrawing CN and Cl groups on DDQ that leads to stabilization of the DDQH$^-$ intermediate. For the DHP/PBQ reaction, this is presumably due to the participation of the nitrogen lone pairs of DHP, which stabilizes the hydropyridinium cation intermediate.

The barriers and the proposed mechanisms of reactions 1, 2, 5, and 6 in various solvents are summarized in Table 16. While the barrier decreases as the solvent becomes more polar for all

four reactions, the largest solvent effect occurs for reaction 6. This is consistent with the mechanism of reaction 6 being ionic or partly ionic for all condensed-phase reactions. Surprisingly, the smallest solvent effect occurs for reaction 2, in which an ionic mechanism is also likely to be the major pathway in the more polar solvents. The relatively modest change in reaction barrier as a function of the solvent polarity for reaction 2, compared with reactions 1 and 5 that are purely radical, is presumably due to insufficient development of charge separation in the transition structure.

3.7. Practical Implications. There are a number of experimental techniques that are used to distinguish a radical mechanism from an ionic mechanism for a reaction or a series of similar reactions. For instance, EPR spectroscopy is widely used for the detection of radicals in a reaction mixture. Likewise, the presence of strong polar effects (as reflected in the effect of substituent or solvent) on reaction rate is commonly used to support an ionic mechanism. The results of the present study suggest that caution should be exercised in reaching such conclusions.

Detection of radicals by EPR would normally be taken to indicate a radical mechanism. However, it cannot rule out a concurrent ionic mechanism. The use of a radical trap introduces another layer of complexity. For example, we have found that in the reaction of acridan with DDQ in the presence of nitrosobenzene, an ionic mechanism seems to be favored over a radical mechanism for the initial hydrogen transfer, despite the detection of radicals by EPR. The apparent contradiction between theory and experiment can be accounted for by proposing that the cationic intermediate is trapped by nitrosobenzene, and that there is subsequent electron transfer to give the radical pair.

Detection of a large solvent effect would normally suggest an ionic mechanism while a small solvent effect might suggest a non-ionic mechanism. However, as illustrated with the CHD/DDQ and DHP/PBQ reactions above, the mechanism of a reaction can change with the solvent. A large solvent effect does not necessarily indicate an ionic mechanism for all solvents but does suggest an ionic mechanism for the more polar solvents. Equally, a small solvent effect may reflect a radical mechanism, or it may reflect an ionic mechanism in which the major part of the charge separation occurs after the transition structure, as illustrated by the CHD/DDQ reaction.

4. Concluding Remarks

A number of important points emerge from the present study.

(1) In the gas phase, all the transfer-hydrogenation reactions examined are predicted to proceed via a radical pathway. The energies of the ion pairs are much higher than those of the radical pairs, and the spin density on the monohydrogenated acceptor increases substantially as the reaction progresses.

(2) The transition structures optimized in the presence of a solvent are found in some cases to differ substantially from the gas-phase geometries. Hence, it is recommended that for theoretical studies of the condensed-phase chemistry, transition structures should be optimized with a solvent.

(3) For the evaluation of solvent effects, we find that the barriers are relatively insensitive to the type of computational method (HF or B3-LYP) and the type of continuum model (IEF-PCM or C-PCM) employed. However, we find that the use of UA0 cavities, in conjunction with UMPWB1K/6-311+G(3df,-2p)//B3-LYP/6-31+G(d,p) gas-phase energies, gives better agreement with experimental barriers than those obtained with UAKS cavities.

(4) The use of a more polar solvent generally leads to an earlier transition structure. Thus, for the reaction $X-H + Y \rightarrow X^{\bullet} + H-Y^{\bullet}$, the breaking $X{\cdots}H$ bond becomes shorter and the forming $H{\cdots}Y$ bond becomes longer as the polarity of the solvent increases. In addition, the barrier generally decreases as the solvent polarity increases. These findings are consistent with the Hammond postulate.

(5) The geometries of the transition structures for the transfer-hydrogenation reactions 1, 2, 5, and 6 show a correlation with the reaction barrier that is in accord with the Hammond postulate. In particular, the breaking bond distances $(X_D{\cdots}H)$ increase with the barrier in an approximately linear fashion.

(6) We find that the gas-phase barriers show a correlation with the energies of the radical intermediates. Thus, the barrier increases in an approximately linear manner as the energy of the intermediates increases. This is consistent with the Bell−Evans−Polanyi principle.

7. For some transfer-hydrogenation reactions with a highly exothermic overall reaction, we find that the second step of the reaction, namely the hydrogen transfer between the intermediates to give the final products, is barrierless.

(8) In some cases, the reaction follows a radical mechanism regardless of the solvent. *However, for some reactions an ionic mechanism becomes the dominant pathway when the solvent is sufficiently polar.* Reactions of this type generally involve substrates that can stabilize the cationic or anionic intermediates. It is of interest to test this scenario experimentally, for example, by the use of trapping agents that would only react with radicals or ions but not both.

(9) Our calculations indicate that the detection of radical adducts by EPR does not necessarily indicate a predominant radical mechanism. This is because the presence of radicals does not rule out a concurrent ionic reaction. In addition, ionic intermediates initially produced from a transfer-hydrogenation reaction may react with the trapping agent to give an ionic adduct, which may subsequently be transformed to a lower energy radical adduct via electron transfer.

(10) For the transfer-hydrogenation reactions examined in the present study, the reaction mechanism varies with the substrate, the substituents, and the solvent. Thus, one should be cautious in utilizing the influence of polar effects on the rate of reaction as a means of determining the mechanism. One must also bear in mind that the rate of reaction depends on the transition structure, which does not necessarily have a strong resemblance to the intermediates.

Supporting Information Available: GAUSSIAN 03 archive entries for B3-LYP/6-31+G(d,p)-optimized geometries of relevant equilibrium and transition structures, calculated MPWB1K/6-311+G(3df,2p) total energies, and calculated free energies of solvation. This material is available free of charge via the Internet at http://pubs.acs.org.

References and Notes

(1) (a) For a comprehensive review on transfer hydrogenations, see: Rüchardt, C.; Gerst, M.; Ebenhoch, J. *Angew. Chem., Int. Ed. Engl.* **1997**, *36*, 1406. See also: (b) Houk, K. N.; Li, Y.; McAllister, M. A.; O'Doherty, G.; Paquette, L. A.; Siebrand, W.; Smedarchina, Z. K. *J. Am. Chem. Soc.* **1994**, *116*, 10895. (c) Mackenzie, K.; Astin, K. B.; Gravett, E. C.; Gregory, R. J.; Howard, J. A. K.; Wilson, C. *J. Phys. Org. Chem.* **1998**, *11*, 879 and references cited therein. (d) Morgenthaler, J.; Rüchardt, C. *Eur. J. Org. Chem.* **1999**, *9*, 2219. (e) Wurche, F.; Sicking, W.; Sustmann, R.; Klarner, F. G.; Rüchardt, C. *Chem. Eur. J.* **2004**, *10*, 2707.

(2) (a) Stein, S. E. *ACS Symp. Ser.* **1981**, *169*, 97. (b) Poutsma, M. L. *Energy Fuels* **1990**, *4*, 113. (c) Adam, W.; Heil, M.; Hutterer, R. *J. Org. Chem.* **1992**, *57*, 4491. (d) Brewster, M. E.; Pop, E.; Huang, M.-J.; Bodor, N. *Heterocycles* **1994**, *37*, 1383. (e) Gebicki, J.; Marcinek, A.; Adamus, J.; Paneth, P.; Rogowski, J. *J. Am. Chem. Soc.* **1996**, *118*, 691. (f) Laarhoven, L. J. J.; Mulder, P. *J. Phys. Chem.* **1997**, *101*, 73.

(3) See, for example: (a) Rylander, P. N. *Hydrogenation over Platinum Metals*; Academic Press: New York, 1967. (b) Jacobsen, E. N.; Pfaltz, A.; Yamamoto, H., Eds. *Comprehensive Asymmetric Catalysis*; Springer: Berlin, Germany, 1999; Vol. 1. (c) Nishimura, S. *Handbook of Heterogeneous Catalytic Hydrogenation for Organic Synthesis*; Wiley: New York, 2001. (d) Genet, J.-P. *Acc. Chem. Res.* **2003**, *36*, 908.

(4) Brumer, Y.; Shapiro, M.; Brumer, P.; Baldridge, K. K. *J. Phys. Chem. A* **2002**, *106*, 9512.

(5) (a) Gerst Rüchardt, C. *Tetrahedron Lett.* **1993**, *34*, 7733. (b) Friebolin, H.; Rüchardt, C. *Liebigs Ann.* **1995**, 1339. (c) Friebolin, H.; Roers, R.; Ebenhoch, J.; Rüchardt, C. *Liebigs Ann.* **1996**, 385.

(6) Wurche, F.; Sicking, W.; Sustmann, R.; Klärner, F.-G.; Rüchardt, C. *Chem. Eur. J.* **2004**, *10*, 2707.

(7) (a) Braude, E. A.; Jackman, L. M.; Linstead, R. P.; Lowe, G. *J. Chem. Soc.* **1960**, 3123 (b) Jackmann, L M. *Adv. Org. Chem.* **1960**, *2*, 329. (c) Trost, B. M. *J. Am. Chem. Soc.* **1967**, *89*, 1847. (d) Stoos, F.; Rocek, J. *J. Am. Chem. Soc.* **1972**, *94*, 27. (e) March, J. *Advanced Organic Chemistry*, 4th ed.; Wiley: New York, 1992; p 1163.

(8) (a) Scott, A. P.; Golding, B. T.; Radom, L. *New J. Chem.* **1998**, 1171. (b) Senger, S.; Radom, S. *J. Phys. Chem. A* **2000**, *104*, 7375. (c) Senger, S.; Radom, L. *J. Am. Chem. Soc.* **2000**, *122*, 2613. (d) Chan, B.; Radom, L. *Aust. J. Chem.* **2004**, *57*, 659. (e) Chan, B.; Radom, L. *J. Am. Chem. Soc.* **2005**, *127*, 2443. (f) Chan. B.; Radom, L. *J. Am. Chem. Soc.* **2006**, *128*, 5322. (g) Miller, D. J.; Smith, D. M.; Chan, B.; Radom, L. *Mol. Phys.* **2006**, *104*, 777. (h) Zhong, G.; Chan. B.; Radom, L. *J. Am. Chem. Soc.* **2007**, *129*, 924. (i) Zhong, G.; Chan. B.; Radom, L. *THEOCHEM* **2007**, *811*, 13.

(9) (a) Koch, W.; Holthausen, M. C. *A Chemist's Guide to Density Functional Theory*, 2nd ed.; Wiley: New York, 2001. (b) Jensen, F. *Introduction to Computational Chemistry*, 2nd ed.; Wiley: Chichester, UK, 2007.

(10) Frisch, M. J.; Trucks, G. W.; Schlegel, H. B.; Scuseria, G. E.; Robb, M. A.; Cheeseman, J. R.; Montgomery, J. A., Jr.; Vreven, T.; Kudin, K. N.; Burant, J. C.; Millam, J. M.; Iyengar, S. S.; Tomasi, J.; Barone, V.; Mennucci, B.; Cossi, M.; Scalmani, G.; Rega, N.; Petersson, G. A.; Nakatsuji, H.; Hada, M.; Ehara, M.; Toyota, K.; Fukuda, R.; Hasegawa, J.; Ishida, M.; Nakajima, T.; Honda, Y.; Kitao, O.; Nakai, H.; Klene, M.; Li, X.; Knox, J. E.; Hratchian, H. P.; Cross, J. B.; Bakken, V.; Adamo, C.; Jaramillo, J.; Gomperts, R.; Stratmann, R. E.; Yazyev, O.; Austin, A. J.; Cammi, R.; Pomelli, C.; Ochterski, J. W.; Ayala, P. Y.; Morokuma, K.; Voth, G. A.; Salvador, P.; Dannenberg, J. J.; Zakrzewski, V. G.; Dapprich, S.; Daniels, A. D.; Strain, M. C.; Farkas, O.; Malick, D. K.; Rabuck, A. D.; Raghavachari, K.; Foresman, J. B.; Ortiz, J. V.; Cui, Q.; Baboul, A. G.; Clifford, S.; Cioslowski, J.; Stefanov, B. B.; Liu, G.; Liashenko, A.; Piskorz, P.; Komaromi, I.; Martin, R. L.; Fox, D. J.; Keith, T.; Al-Laham, M. A.; Peng, C. Y.; Nanayakkara, A.; Challacombe, M.; Gill, P. M. W.; Johnson, B.; Chen, W.; Wong, M. W.; Gonzalez, C.; Pople, J. A. *Gaussian 03*, Revision D.01; Gaussian, Inc.: Wallingford, CT, 2004.

(11) Zhao, Y.; Truhlar, D. G. *J. Phys. Chem. A* **2004**, *108*, 6908.

(12) (a) Cremer, D.; Filatov, M.; Polo, V.; Kraka, E.; Shaik, S. *Int. J. Mol. Sci.* **2002**, *3*, 604. (b) Polo, V.; Gräfenstein, J.; Kraka, E.; Cremer, D. *Theor. Chem. Acc.* **2003**, *109*, 22. (c) Schreiner, P. R.; Navarro-Vazquez, A.; Prall, M. *Acc. Chem. Res.* **2005**, *38*, 29.

(13) See, for example: Chen, W.; Schlegel, H. B. *J. Chem. Phys.* **1994**, *101*, 5957.

(14) See ref 9a, pp 52−54, and references cited therein.

(15) Löwdin, P. O. *Phys. Rev.* **1995**, *97*, 1474.

(16) Gräfenstein, J.; Cremer, D. *Mol. Phys.* **2001**, *99*, 981.

(17) Scott, A. P.; Radom, L. *J. Phys. Chem.* **1996**, *100*, 16502.

(18) Mulliken, R. S. *J. Chem. Phys.* **1955**, *23*, 1833.

(19) (a) Cancès, M. T.; Mennucci, B.; Tomasi, J. *J. Chem. Phys.* **1997**, *107*, 3032. (b) Mennucci, B.; Tomasi, J. *J. Chem. Phys.* **1997**, *106*, 5151. (c) Mennucci, B.; Cancès, E.; Tomasi, J. *J. Phys. Chem. B* **1997**, *101*, 10506. (d) Tomasi, J.; Mennucci, B.; Cancès, E. *THEOCHEM* **1999**, *464*, 211.

(20) (a) Barone, V.; Cossi, M. *J. Phys. Chem. A* **1998**, *102*, 1995. (b) Cossi, M.; Rega, N.; Scalmani, G.; Barone, V. *J. Comput. Chem.* **2003**, *24*, 669.

(21) Barone, V.; Cossi, M.; Tomasi, J. *J. Chem. Phys.* **1997**, *107*, 3210.

(22) Rappé, A. K.; Casewit, C. J.; Colwell, K. S.; Goddard, W. A., III; Skiff, W. M. *J. Am. Chem. Soc.* **1992**, *114*, 10024.

(23) (a) Massova, I.; Kollman, P. A. *J. Phys. Chem. B* **1999**, *103*, 8628. (b) Takano, Y.; Houk, K. N. *J. Chem. Theory Comput.* **2005**, *1*, 70.

(24) Hammond, G. S. *J. Am. Chem. Soc.* **1955**, *77*, 334.

(25) Höller, C.; Rüchardt, C. *Liebigs Ann.* **1996**, 183.

(26) We note that the point for reaction 1, which is the only one of the four reactions that does not involve quinones as acceptors, deviates somewhat from ideal BEP behavior.

(27) (a) Bell, R. P. *Proc. R. Soc. A* **1936**, *154*, 414. (b) Evans, M. G.; Polanyi, M. *Trans. Faraday Soc.* **1938**, *34*, 11.